

An Analytical Method to Obtain Maximum Allowable Grid Support by Using Grid-Connected Converters

Masoud M. Shabestary, *Student Member, IEEE*, and Yasser Abdel-Rady I. Mohamed, *Senior Member, IEEE*

Abstract—Recently, supporting the grid voltage and proper operation of the grid-connected converters (GCCs) under a wide range of grid voltage conditions have become major requirements. An analytical study is very useful for evaluating the supporting capability of the available control strategies in GCCs. This paper analytically studies, then modifies the supporting capability of three existing strategies. The contribution of this paper is two-fold: first, analytical expressions of instantaneous active/reactive powers oscillation and maximum phase currents are formulated and used to conduct several comparisons among different strategies. Second, based on the obtained formulas for the maximum phase currents, maximum allowable support (MAS) control schemes are proposed under unbalanced voltage conditions. The MAS control schemes have two important objectives: obtaining maximum active or reactive power delivery and simultaneously respecting the maximum phase currents under the unbalanced condition. The proposed equations can further estimate the maximum depth of the faulted voltage where each strategy is still able to satisfy the voltage support requirements imposed by the grid codes. The proposed expressions can also help all techniques to provide their maximum voltage or frequency support under the pre-set maximum phase current limitations. Different selected simulation and experimental tests are carried out for comparing the strategies, and validating the effectiveness of the proposed MAS equations.

Index Terms—Grid faults, low voltage ride through (LVRT), maximum allowable grid support, maximum fault current, positive and negative sequence currents, power converters, reference current generation, unbalanced faults.

NOMENCLATURE

V^+	Magnitude of positive-sequence of the point of common coupling (PCC) voltage.
V^-	Magnitude of negative-sequence of PCC voltage.
v_\perp	Orthogonal voltage vector (90° leading from v).
$\tilde{p}(\tilde{q})$	Active (reactive) power oscillatory terms.
$\tilde{p}_{s2}(\tilde{q}_{s2})$	Active (reactive) power oscillation terms oscillating by $\sin(2\omega t)$.
$\tilde{p}_{c2}(\tilde{q}_{c2})$	Active (reactive) power oscillation terms oscillating by $\cos(2\omega t)$.
$P_{s2}(P_{c2})$	Magnitude of $\tilde{p}_{s2}(\tilde{p}_{c2})$.
$Q_{s2}(Q_{c2})$	Magnitude of $\tilde{q}_{s2}(\tilde{q}_{c2})$.
I_{\max}	Maximum of three phase currents under the fault.
I_{limit}	Imposed Limitation for I_{\max} .

Manuscript received September 14, 2015; revised December 16, 2015 and April 8, 2016; accepted May 11, 2016. Date of publication May 13, 2016; date of current version October 7, 2016. Paper number TSTE-00773-2015.

The authors are with the Department of Electrical and Computer Engineering, University of Alberta, Edmonton, AB T6G-2V4, Canada (e-mail: masoud2@ualberta.ca; yasser2@ualberta.ca).

Color versions of one or more of the figures in this paper are available online at <http://ieeexplore.ieee.org>.

Digital Object Identifier 10.1109/TSTE.2016.2569022

I. INTRODUCTION

GLOBAL energy statistics clearly show the booming share of renewable energy resource and distributed generation (DG) units in the overall generation mix, and the trend is set to continue at an even considerably higher pace in the future. This growing participation has created serious stability concerns [1]. As a result, system operators in different countries have been releasing stringent requirements for the operation of the grid-connected converters (GCCs) under abnormal grid conditions [2]. According to these codes, GCCs are required to keep feeding the grid and to provide voltage/frequency supports during abnormal conditions [3], [4]. These requirements and the compliance of the newly developed generation units have been extensively studied in the literature, as, for example, in [5]–[25]. Different control strategies have been proposed in [13]–[25] for GCCs which are also the focus of this paper.

Depending on the aim of the control strategy used to generate the reference currents under abnormal conditions, the general performance of the converter and its interaction with the grid will vary significantly [21]. Consequently, the reference current generation (RCG) is a challenging issue in the control of GCCs [22]. Under unbalanced voltages, the currents injected into the grid may become non-sinusoidal and/or unbalanced. Such currents and voltages may lead to undesired fluctuations in the active and reactive power injected into the grid. The appropriate operation of the GCC under such conditions is another critical issue [21].

In order to compare different RCG strategies comprehensively, their thorough analytical evaluation and precise mathematical assessment are necessary. This paper initially presents a detailed comparative study and evaluation results of three available RCG strategies (proposed in [21], [22]), and then presents further analytical expressions to characterize their performances. The analytical study and the proposed ideas in this paper can be also expanded to other RCG strategies proposed by [23]–[25]. These evaluations will help engineers to design proper control schemes for the GCCs. This paper introduces the three most important terms for analytical evaluations and reasonable comparisons. Maximum oscillations on active/reactive powers (\tilde{p}_{\max} and \tilde{q}_{\max}) and I_{\max} are the three most important terms for evaluating RCG strategies. The mathematical equations of \tilde{p}_{\max} , \tilde{q}_{\max} and I_{\max} for these strategies are calculated in this paper.

As the main contribution of this work, the maximum allowable support (MAS) control schemes are proposed based on the obtained expressions of I_{\max} . The obtained I_{\max} equations are

useful for calculating the maximum allowable active or reactive powers which the converter can deliver to the grid under abnormal grid conditions (in order to support either the grid voltage or the grid frequency) without exceeding the maximum phase current limit, I_{limit} . Therefore, the MAS control schemes have two goals: (i) to provide the maximum support for the grid voltage and/or frequency and, simultaneously, (ii) to respect the phase currents maximum limit imposed by the GCC ratings. The mathematical equations of the MAS control schemes under various conditions for the three strategies are obtained and presented in Section V. One of the best features of the MAS equations is their ability to estimate the maximum voltage depth where each strategy is still capable to successfully meet the voltage support requirements of the grid codes. The obtained analytical expressions are validated by selected simulation and experimental test cases in Sections VI and VII. These test cases also verify the effectiveness of the proposed MAS control schemes.

II. RCG STRATEGIES

In this section, three strategies (introduced in [21], [22]) are presented to generate the reference-currents in order to uninterrupted deliver the required active/reactive powers under the grid faults. Each of these strategies demonstrates a specific performance. According to the instantaneous power theories [26], the active power, P , can be obtained by a current vector aligned with the voltage vector, v , while a current vector aligned with v_{\perp} results in the reactive power, Q . Therefore, the reference active/reactive currents, i_p^* and i_q^* , are given by (1) in order to deliver P and Q

$$i_p^* = g v, \quad i_q^* = b v_{\perp} \quad (1)$$

where g and b can be considered as instantaneous conductance and instantaneous susceptance [21]. The total reference-current is obtained by

$$i^* = i_p^* + i_q^* = i_{p+}^* + i_{p-}^* + i_{q+}^* + i_{q-}^*. \quad (2)$$

To obtain the required P and Q , g and b can be defined as

$$\begin{aligned} P^* &= i_p^* \cdot v = g v \cdot v = g |v|^2 \Rightarrow g = \frac{P^*}{|v|^2} \\ Q^* &= i_q^* \cdot v = b v_{\perp} \cdot v = b |v|^2 \Rightarrow b = \frac{Q^*}{|v|^2}. \end{aligned} \quad (3)$$

Under balanced sinusoidal grid voltages, the reference-currents given by (1) and (3) are sinusoidal. However, under unbalanced voltages, the module $|v|^2$ contains oscillations at twice the fundamental frequency (ω) as

$$|v|^2 = |v^+|^2 + |v^-|^2 + 2|v^+||v^-|\cos(2\omega t + \delta^+ - \delta^-) \quad (4)$$

where v^+ and v^- are, respectively, the positive and negative voltage vectors of the PCC. According to (4), the obtained reference-currents can be non-sinusoidal and contain harmonics under the unbalanced voltage condition. These distorted currents have several drawbacks such as requiring complicated controllers, overcurrent problems, excitation of resonances, and extra deterioration of the PCC voltage.

A. Balanced Positive-Sequence Control (BPSC) [21]–[33]

If the quality of the injected currents is important, then the reference currents should be not only sinusoidal, but also balanced. Therefore, g and b can be obtained by

$$\begin{aligned} i_p^* &= g_{\text{BPSC}} v^+, \quad g_{\text{BPSC}} = \frac{P^*}{|v^+|^2} \\ i_q^* &= b_{\text{BPSC}} v_{\perp}^+, \quad b_{\text{BPSC}} = \frac{Q^*}{|v^+|^2}. \end{aligned} \quad (5)$$

Equation (5) implies that the reference-currents are sinusoidal and balanced even under unbalanced conditions since they follow only the positive sequence of the PCC voltage.

B. Instantaneously-Controlled Positive Sequence (ICPS) [22]

Reference [22] introduces the ICPS strategy which delivers P and Q by following g and b :

$$\begin{aligned} i_p^* &= g_{\text{ICPS}} v^+, \quad g_{\text{ICPS}} = \frac{P^*}{|v^+|^2 + v^+ \cdot v^-} \\ i_q^* &= b_{\text{ICPS}} v_{\perp}^+, \quad b_{\text{ICPS}} = \frac{Q^*}{|v^+|^2 + v^+ \cdot v^-}. \end{aligned} \quad (6)$$

By using this strategy, non-sinusoidal and unbalanced reference-currents are generated under unbalanced conditions since g_{ICPS} and b_{ICPS} calculated by (6) have oscillations in their denominators at twice the fundamental frequency. The detailed derivation of the ICPS currents in the *abc* frame is given in the next section. According to the obtained equations, these currents are in the forms of

$$i_a^{\text{ICPS}} = \frac{P \cos(\omega t) - Q \sin(\omega t)}{V^+ - V^- \cos(2\omega t)} \quad (7)$$

$$i_b^{\text{ICPS}} = \frac{(\frac{-1}{2}P + \frac{\sqrt{3}}{2}Q) \cos(\omega t) + (\frac{\sqrt{3}}{2}P + \frac{1}{2}Q) \sin(\omega t)}{V^+ - V^- \cos(2\omega t)} \quad (8)$$

$$i_c^{\text{ICPS}} = \frac{(\frac{-1}{2}P - \frac{\sqrt{3}}{2}Q) \cos(\omega t) + (\frac{-\sqrt{3}}{2}P + \frac{1}{2}Q) \sin(\omega t)}{V^+ - V^- \cos(2\omega t)}. \quad (9)$$

From (7) to (9), the *abc* currents in the ICPS strategy can be found to contain harmonics due to the oscillatory terms in the denominators of the *abc* currents. Unbalances and harmonics in the currents may lead to over-current issues, as mentioned earlier.

C. Positive and Negative Sequence Control (PNSC) [21], [22]

As another approach, the PNCS strategy calculates a reference-current vector which contains a proper set of positive- and negative-sequence components and aims to remove some oscillation terms in the instantaneous active and reactive powers. According to the instantaneous power theories [26], the

instantaneous active/reactive powers are as follows:

$$\begin{aligned} p = & \underbrace{v^+ \cdot i_p^{*+} + v^- \cdot i_p^{*-}}_P + \underbrace{v^+ \cdot i_q^{*+} + v^- \cdot i_q^{*-}}_0 \\ & + \boxed{\underbrace{v^+ \cdot i_p^{*-} + v^- \cdot i_p^{*+}}_{\tilde{p}_{c2}} + \underbrace{v^+ \cdot i_q^{*-} + v^- \cdot i_q^{*+}}_{\tilde{p}_{s2}}} \quad (10) \end{aligned}$$

$$\begin{aligned} q = & \underbrace{v_\perp^+ \cdot i_q^{*+} + v_\perp^- \cdot i_q^{*-}}_Q + \underbrace{v_\perp^+ \cdot i_p^{*+} + v_\perp^- \cdot i_p^{*-}}_0 \\ & + \boxed{\underbrace{v_\perp^+ \cdot i_q^{*-} + v_\perp^- \cdot i_q^{*+}}_{\tilde{q}_{c2}} + \underbrace{v_\perp^+ \cdot i_p^{*-} + v_\perp^- \cdot i_p^{*+}}_{\tilde{q}_{s2}}}. \quad (11) \end{aligned}$$

Reference [21] proposes to cancel out the summation of the fifth and sixth terms of both the active and reactive powers bordered in (10), (11), respectively. Thus, the reference currents can be obtained as

$$\begin{aligned} i_p^* &= g_{\text{PNSC}}(v^+ - v^-), \quad g_{\text{PNSC}} = \frac{P^*}{|v^+|^2 - |v^-|^2} \\ i_q^* &= b_{\text{PNSC}}(v_\perp^+ - v_\perp^-), \quad b_{\text{PNSC}} = \frac{Q^*}{|v^+|^2 - |v^-|^2}. \quad (12) \end{aligned}$$

III. MATHEMATICAL EQUATIONS OF INSTANTANEOUS ACTIVE/REACTIVE POWER OSCILLATION TERMS

In this section, the equations of \tilde{p}_{\max} and \tilde{q}_{\max} for the three strategies are presented. According to [21], the equations of the instantaneous active/reactive powers are in the forms of

$$\begin{aligned} p &= v \cdot i = (v^+ + v^-) \cdot (i^+ + i^-) = \underbrace{v^+ \cdot i^+ + v^- \cdot i^-}_P \\ &\quad + \underbrace{v^+ \cdot i^- + v^- \cdot i^+}_{\tilde{p}} \\ &= P + \tilde{p}_{s2} + \tilde{p}_{c2} = P + P_{s2} \sin(2\omega t) + P_{c2} \cos(2\omega t) \quad (13) \end{aligned}$$

$$\begin{aligned} q &= v_\perp \cdot i = (v_\perp^+ + v_\perp^-) \cdot (i^+ + i^-) = \underbrace{v_\perp^+ \cdot i^+ + v_\perp^- \cdot i^-}_Q \\ &\quad + \underbrace{v_\perp^+ \cdot i^- + v_\perp^- \cdot i^+}_{\tilde{q}} \\ &= Q + \tilde{q}_{s2} + \tilde{q}_{c2} = Q + Q_{s2} \sin(2\omega t) + Q_{c2} \cos(2\omega t). \quad (14) \end{aligned}$$

Expressions of \tilde{p} and \tilde{q} are provided for the PNSC strategy in [21]. However, the obtained expressions in [21] for the BPSC strategy are not correct. Moreover, [22] has no \tilde{p} expression for the ICPS. In fact, the expressions of their maximum oscillation values, i.e., \tilde{p}_{\max} and \tilde{q}_{\max} , are more useful for their evaluation. Hence, this paper finds the expressions of \tilde{p}_{\max} and \tilde{q}_{\max} . Also, representing the expressions of \tilde{p}_{\max} and \tilde{q}_{\max} in terms of the scalar parameters is more desirable.

By neglecting initial voltage angles, the positive and negative sequences of the voltage vector and their orthogonal forms for the single phase unbalanced condition can be simply written in the $\alpha\beta$ frame as [32]

$$v^+ = \begin{bmatrix} V^+ \cos(\omega t) \\ V^+ \sin(\omega t) \end{bmatrix} \quad (15)$$

$$v_\perp^+ = \begin{bmatrix} -V^+ \sin(\omega t) \\ V^+ \cos(\omega t) \end{bmatrix} \quad (16)$$

$$v^- = \begin{bmatrix} -V^- \cos(\omega t) \\ V^- \sin(\omega t) \end{bmatrix} \quad (17)$$

$$v_\perp^- = \begin{bmatrix} -V^- \sin(\omega t) \\ -V^- \cos(\omega t) \end{bmatrix}. \quad (18)$$

By using (15)–(18) in (10)–(12), the instantaneous active/reactive powers of the PNSC strategy can be obtained as

$$\begin{aligned} p &= \underbrace{v^+ \cdot i_p^+ + v^- \cdot i_p^-}_P + \underbrace{v^+ \cdot i_q^- + v^- \cdot i_q^+}_{\tilde{p}_{s2}} \\ &= P + \frac{2QV^+V^- \sin(2\omega t)}{(V^+)^2 - (V^-)^2} \quad (19) \end{aligned}$$

$$\begin{aligned} q &= \underbrace{v_\perp^+ \cdot i_q^+ + v_\perp^- \cdot i_q^-}_Q + \underbrace{v_\perp^+ \cdot i_p^- + v_\perp^- \cdot i_p^+}_{\tilde{q}_{s2}} \\ &= Q - \frac{2PV^+V^- \sin(2\omega t)}{(V^+)^2 - (V^-)^2}. \quad (20) \end{aligned}$$

Thus, \tilde{p}_{\max} and \tilde{q}_{\max} of the PNSC strategy are

$$\tilde{p}_{\max}^{\text{PNSC}} = \frac{2nQ}{1-n^2}; \quad \tilde{q}_{\max}^{\text{PNSC}} = \frac{2nP}{1-n^2} \quad (21)$$

where n is defined as the ratio of the negative voltage magnitude over the positive voltage magnitude (i.e., $n = \frac{V^-}{V^+}$), which is a characteristic of the unbalanced voltage condition.

By applying (5) in (13)–(14), instantaneous active and reactive powers of the BPSC can be written:

$$\begin{aligned} p &= v \cdot (i_p + i_q) = (v^+ + v^-) \cdot \left(\frac{P}{(V^+)^2} v^+ + \frac{Q}{(V^+)^2} v_\perp^+ \right) = \\ &= P + \frac{Q}{(V^+)^2} v^+ \cdot v_\perp^+ + \frac{P}{(V^+)^2} (v^+ \cdot v^-) + \frac{Q}{(V^+)^2} (v^- \cdot v_\perp^+) \\ &= P - n \cdot P \cdot \cos(2\omega t) + n \cdot Q \cdot \sin(2\omega t) \quad (22) \end{aligned}$$

$$q = v_\perp \cdot (i_p + i_q) = Q - n \cdot Q \cdot \cos(2\omega t) - n \cdot P \cdot \sin(2\omega t). \quad (23)$$

Thus, \tilde{p}_{\max} and \tilde{q}_{\max} of the BPSC strategy can be given by

$$\tilde{p}_{\max}^{\text{BPSC}} = \tilde{q}_{\max}^{\text{BPSC}} = n \cdot \sqrt{P^2 + Q^2}. \quad (24)$$

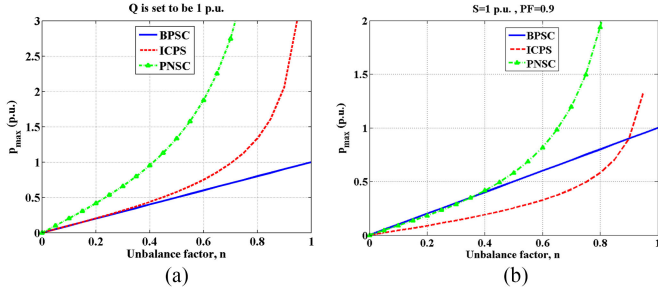


Fig. 1. \tilde{p}_{\max} values of three strategies for all possible n values when (a) $Q = 1$ p.u. and $P = 0$ p.u. (supporting PCC voltage and curtailing the active power), and (b) $P = 0.9$ p.u. and $Q = \sqrt{S^2 - P^2} = 0.44$ p.u. (continuing the active power delivery).

Finally, (25) and (26) provide the instantaneous active and reactive powers of the ICPS strategy as

$$\begin{aligned} p &= v \cdot i = (v^+ + v^-) \cdot (i_p^+ + i_q^+) \\ &= P + Q \frac{v^- \cdot v_\perp^+}{(V^+)^2 + v^+ \cdot v^-} \end{aligned} \quad (25)$$

$$\begin{aligned} q &= v_\perp \cdot i = (v_\perp^+ + v_\perp^-) \cdot (i_p^+ + i_q^+) \\ &= Q + P \frac{v_\perp^+ \cdot v^+}{(V^+)^2 + v^+ \cdot v^-}. \end{aligned} \quad (26)$$

Applying (15)–(18) in (25), (26) gives

$$\begin{aligned} p &= P + \frac{Q V^- \sin(2\omega t)}{V^+ - V^- \cos(2\omega t)} \\ q &= Q + \frac{-P V^- \sin(2\omega t)}{V^+ - V^- \cos(2\omega t)}. \end{aligned} \quad (27)$$

Hence, \tilde{p}_{\max} and \tilde{q}_{\max} of the ICPS strategy can be obtained:

$$\tilde{p}_{\max}^{\text{ICPS}} = \frac{nQ}{\sqrt{1-n^2}}, \quad \tilde{q}_{\max}^{\text{ICPS}} = \frac{nP}{\sqrt{1-n^2}}. \quad (28)$$

The analytical expressions of maximum oscillations on the instantaneous active/reactive power are presented in this section. For a visual comparison, two diagrams of Fig. 1 are depicted, based on (21), (24), and (28), to show the value of \tilde{p}_{\max} 's in two different sets of P and Q values and all possible n values. Fig. 1 indicates the performances of the three strategies in terms of \tilde{p}_{\max} under a wide range of fault cases. Based on the obtained expressions and Fig. 1, some useful conclusions can be made:

- 1) \tilde{p}_{\max} and \tilde{q}_{\max} in both the ICPS and PNSC strategies depend on their anti-corresponding power components (i.e. \tilde{p}_{\max} depends on the average reactive power, whereas \tilde{q}_{\max} depends on the average active power). The comparison between (21) and (28) shows that the \tilde{p}_{\max} value in the ICPS strategy is theoretically less than half of the \tilde{p}_{\max} value in the PNSC strategy.
- 2) In high power factors, the ICPS strategy has the lowest oscillations on the active power among the three strategies (compare (21) with (24) and (28), and see Fig. 1(b)). This result is due to the dependency of \tilde{p}_{\max} on Q in this strategy. This diagram reveals a range for n where the ICPS strategy has the lowest oscillation on the active power.

Therefore, the ICPS strategy can be desirable, in higher power factors, for the cases where the dc-link controller is more vulnerable.

- 3) In the unity power factor operation, the PNSC strategy has no oscillation on p , but causes the highest oscillations on p and q , in low power factors and high unbalanced conditions (see (21) and Fig. 1). This figure reveals that the PNSC strategy is not recommended for the cases that dc-voltage controller is vulnerable under active power oscillations.
- 4) In the BPSC strategy, \tilde{p}_{\max} and \tilde{q}_{\max} are equal and depend on both the active and reactive power values. Therefore, \tilde{p}_{\max} and \tilde{q}_{\max} of the BPSC can be higher or lower than those of the other two strategies depending on the P , Q and n . However, the \tilde{p}_{\max} and \tilde{q}_{\max} values of the BPSC are always lower than 1 p.u. based on (24), unlike these values in the other two strategies (see Fig. 1 for comparisons). This feature makes the BPSC strategy a reliable option when the active and reactive powers oscillations are important. The acceptable thresholds of these oscillations can be also easily controlled since the oscillations have linear relationships with the unbalance factor.

IV. MATHEMATICAL EXPRESSIONS OF MAXIMUM INSTANTANEOUS PHASE CURRENTS

According to [21] and [32], for any unbalanced condition, the positive and negative sequence voltage vectors and their orthogonal forms can be written in the $\alpha\beta$ frame as

$$\begin{aligned} v^+ &= \begin{bmatrix} v_\alpha^+ \\ v_\beta^+ \end{bmatrix} = \begin{bmatrix} V^+ \cos(\omega t + \delta^+) \\ V^+ \sin(\omega t + \delta^+) \end{bmatrix} \\ v_\perp^+ &= \begin{bmatrix} -v_\beta^+ \\ v_\alpha^+ \end{bmatrix} = \begin{bmatrix} -V^+ \sin(\omega t + \delta^+) \\ V^+ \cos(\omega t + \delta^+) \end{bmatrix} \\ v^- &= \begin{bmatrix} v_\alpha^- \\ v_\beta^- \end{bmatrix} = \begin{bmatrix} V^- \cos(\omega t + \delta^-) \\ -V^- \sin(\omega t + \delta^-) \end{bmatrix} \\ v_\perp^- &= \begin{bmatrix} -v_\beta^- \\ v_\alpha^- \end{bmatrix} = \begin{bmatrix} V^- \sin(\omega t + \delta^-) \\ V^- \cos(\omega t + \delta^-) \end{bmatrix} \end{aligned} \quad (29)$$

where δ^+ and δ^- are, respectively, the phase angles of the positive and negative sequence voltages.

A. Maximum Phase Currents in BPSC

Applying the positive sequence terms of (29) in (5) gives

$$\begin{aligned} i_{\text{BPSC}} &= \begin{bmatrix} i_\alpha^{\text{BPSC}} \\ i_\beta^{\text{BPSC}} \end{bmatrix} = g_{\text{BPSC}} \begin{bmatrix} V^+ \cos(\lambda^+) \\ V^+ \sin(\lambda^+) \end{bmatrix} \\ &\quad + b_{\text{BPSC}} \begin{bmatrix} -V^+ \sin(\lambda^+) \\ V^+ \cos(\lambda^+) \end{bmatrix} \end{aligned} \quad (30)$$

where $\lambda^+ = \omega t + \delta^+$. Applying g_{BPSC} and b_{BPSC} from (5) in (30) results in

$$\begin{bmatrix} i_a^{\text{BPSC}} \\ i_b^{\text{BPSC}} \\ i_c^{\text{BPSC}} \end{bmatrix} = \frac{1}{V^+} \begin{bmatrix} P \cos(\lambda^+) - Q \sin(\lambda^+) \\ P \sin(\lambda^+) + Q \cos(\lambda^+) \end{bmatrix}. \quad (31)$$

To find the maximum phase currents in the *abc* frame, the $\alpha\beta$ components should be transformed into *abc* components by using

$$\begin{bmatrix} i_a \\ i_b \\ i_c \end{bmatrix} = \begin{bmatrix} 1 & 0 \\ -\frac{1}{2} & \frac{\sqrt{3}}{2} \\ -\frac{1}{2} & -\frac{\sqrt{3}}{2} \end{bmatrix} \cdot \begin{bmatrix} i_\alpha \\ i_\beta \end{bmatrix} \rightarrow$$

$$\begin{bmatrix} |i_a| \\ |i_b| \\ |i_c| \end{bmatrix} = \begin{bmatrix} |i_\alpha| \\ \left| -\frac{1}{2}i_\alpha + \frac{\sqrt{3}}{2}i_\beta \right| \\ \left| \frac{1}{2}i_\alpha + \frac{\sqrt{3}}{2}i_\beta \right| \end{bmatrix}. \quad (32)$$

Applying (32) in (31) gives

$$\begin{aligned} & \begin{bmatrix} i_a^{\text{BPSC}} \\ i_b^{\text{BPSC}} \\ i_c^{\text{BPSC}} \end{bmatrix} \\ &= \begin{bmatrix} \frac{P \cos(\lambda^+) - Q \sin(\lambda^+)}{V^+} \\ \frac{\left(\frac{-1}{2}P + \frac{\sqrt{3}}{2}Q \right) \cos(\lambda^+) + \left(\frac{\sqrt{3}}{2}P + \frac{1}{2}Q \right) \sin(\lambda^+)}{V^+} \\ \frac{\left(\frac{-1}{2}P - \frac{\sqrt{3}}{2}Q \right) \cos(\lambda^+) + \left(\frac{-\sqrt{3}}{2}P + \frac{1}{2}Q \right) \sin(\lambda^+)}{V^+} \end{bmatrix} \\ &= \begin{bmatrix} \frac{\sqrt{P^2 + Q^2}}{V^+} \cos\left(\lambda^+ + \tan^{-1}\frac{Q}{P}\right) \\ \frac{\sqrt{P^2 + Q^2}}{V^+} \cos\left(\lambda^+ + \tan^{-1}\frac{Q}{P} - \frac{2\pi}{3}\right) \\ \frac{\sqrt{P^2 + Q^2}}{V^+} \cos\left(\lambda^+ + \tan^{-1}\frac{Q}{P} + \frac{2\pi}{3}\right) \end{bmatrix}. \quad (33) \end{aligned}$$

Therefore, the magnitude of the *abc* currents and the maximum current are obtained as

$$I_{\max-BPSC} = |i_a^{\text{BPSC}}| = |i_b^{\text{BPSC}}| = |i_c^{\text{BPSC}}| = \frac{\sqrt{P^2 + Q^2}}{V^+}. \quad (34)$$

B. Maximum Phase Currents in PNSC

The reference current of the PNSC strategy is obtained in the $\alpha\beta$ frame by

$$\begin{aligned} i^{\text{PNSC}} = & \begin{bmatrix} i_\alpha^{\text{PNSC}} \\ i_\beta^{\text{PNSC}} \end{bmatrix} = g_{\text{PNSC}} (v^+ - v^-) \\ & + b_{\text{PNSC}} \cdot (v_\perp^+ - v_\perp^-). \end{aligned} \quad (35)$$

Applying (29) in (35) gives

$$\begin{aligned} & \begin{bmatrix} i_\alpha^{\text{PNSC}} \\ i_\beta^{\text{PNSC}} \end{bmatrix} = g_{\text{PNSC}} \begin{bmatrix} V^+ \cos(\lambda^+) - V^- \cos(\lambda^-) \\ V^+ \sin(\lambda^+) + V^- \sin(\lambda^-) \end{bmatrix} \\ & + b_{\text{PNSC}} \begin{bmatrix} -V^+ \sin(\lambda^+) - V^- \sin(\lambda^-) \\ V^+ \cos(\lambda^+) - V^- \cos(\lambda^-) \end{bmatrix} \end{aligned} \quad (36)$$

where $\lambda^+ = \omega t + \delta^+$ and $\lambda^- = \omega t + \delta^-$.

According to [32], if the faulted phase is *a*, then the value of $(\delta^+ - \delta^-)$ is π . It can be theoretically proven that assuming that other phases are faulted will not change the final results. In fact, it will change only the order of the three obtained expressions. Therefore, if phase *a* is assumed to be the faulted phase, the current magnitude of the three phases can be calculated by considering $\delta^+ - \delta^- = \lambda^+ - \lambda^- = \pi$. Thus, (36) can be rewritten for the faulted phase *a* as

$$\begin{aligned} & \begin{bmatrix} i_a^{F,a} \\ i_\beta^{F,a} \end{bmatrix} = g_{\text{PNSC}} \begin{bmatrix} (V^+ + V^-) \cos(\lambda^+) \\ (V^+ - V^-) \sin(\lambda^+) \end{bmatrix} \\ & + b_{\text{PNSC}} \begin{bmatrix} (-V^+ + V^-) \sin(\lambda^+) \\ (V^+ + V^-) \cos(\lambda^+) \end{bmatrix} \\ &= g_{\text{PNSC}} \begin{bmatrix} V_2 \cos(\lambda^+) \\ V_1 \sin(\lambda^+) \end{bmatrix} + b_{\text{PNSC}} \begin{bmatrix} -V_1 \sin(\lambda^+) \\ V_2 \cos(\lambda^+) \end{bmatrix} \end{aligned} \quad (37)$$

where $V_1 = V^+ - V^-$ and $V_2 = V^+ + V^-$, and superscript “*F, a*” stands for the case in which phase *a* is faulted. Applying (32) in (37) gives the *abc* currents as (38) shown at the bottom of the page.

$$\begin{bmatrix} i_a^{F,a} \\ i_b^{F,a} \\ i_c^{F,a} \end{bmatrix} = \begin{bmatrix} g_{\text{PNSC}} V_2 \cos(\lambda^+) - b_{\text{PNSC}} V_1 \sin(\lambda^+) \\ \left(\frac{-1}{2}g_{\text{PNSC}} + \frac{\sqrt{3}}{2}b_{\text{PNSC}} \right) V_2 \cos(\lambda^+) + \left(\frac{\sqrt{3}}{2}g_{\text{PNSC}} + \frac{1}{2}b_{\text{PNSC}} \right) V_1 \sin(\lambda^+) \\ \left(\frac{-1}{2}g_{\text{PNSC}} - \frac{\sqrt{3}}{2}b_{\text{PNSC}} \right) V_2 \cos(\lambda^+) + \left(\frac{-\sqrt{3}}{2}g_{\text{PNSC}} + \frac{1}{2}b_{\text{PNSC}} \right) V_1 \sin(\lambda^+) \end{bmatrix}. \quad (38)$$

Applying the equivalents of g_{PNSC} and b_{PNSC} in (38) and calculating the magnitude of each phase results in

$$\begin{bmatrix} |i_a^{F,a}| \\ |i_b^{F,a}| \\ |i_c^{F,a}| \end{bmatrix} = \frac{1}{(V^+)^2 - (V^-)^2} \begin{bmatrix} \sqrt{N^2 + 2V^+V^-(P^2 - Q^2)} \\ \sqrt{N^2 + V^+V^-(Q^2 - P^2 - 2\sqrt{3}PQ)} \\ \sqrt{N^2 + V^+V^-(Q^2 - P^2 + 2\sqrt{3}PQ)} \end{bmatrix} \quad (39)$$

where $N^2 = P^2(V^+)^2 + P^2(V^-)^2 + Q^2(V^+)^2 + Q^2(V^-)^2$.

For a fault in phase b , $\delta^+ - \delta^-$ is $\pi/3$ [32]. Therefore, it is assumed that $\delta^+ - \delta^- = \lambda^+ - \lambda^- = \pi/3$ in (36) in order to obtain the expressions of the PNSC currents for a fault in phase b :

$$\begin{bmatrix} i_\alpha^{F,b} \\ i_\beta^{F,b} \\ i_\gamma^{F,b} \end{bmatrix} = g_{\text{PNSC}} \begin{bmatrix} V^+ \cos(\lambda^+) - V^- \cos\left(\lambda^+ - \frac{\pi}{3}\right) \\ V^+ \sin(\lambda^+) + V^- \sin\left(\lambda^+ - \frac{\pi}{3}\right) \end{bmatrix} + b_{\text{PNSC}} \begin{bmatrix} -V^+ \sin(\lambda^+) - V^- \sin\left(\lambda^+ - \frac{\pi}{3}\right) \\ V^+ \cos(\lambda^+) - V^- \cos\left(\lambda^+ - \frac{\pi}{3}\right) \end{bmatrix} \quad (40)$$

where superscript “ F, b ” stands for the case in which phase b is faulted. (40) can be simplified as

$$\begin{bmatrix} i_\alpha^{F,b} \\ i_\beta^{F,b} \end{bmatrix} = \begin{bmatrix} I_{\alpha,c} \cos(\lambda^+) + I_{\alpha,s} \sin(\lambda^+) \\ I_{\beta,c} \cos(\lambda^+) + I_{\beta,s} \sin(\lambda^+) \end{bmatrix} \quad (41)$$

where

$$\begin{bmatrix} I_{\alpha,c} \\ I_{\alpha,s} \\ I_{\beta,c} \\ I_{\beta,s} \end{bmatrix} = \begin{bmatrix} g_{\text{PNSC}}V^+ - \frac{1}{2}g_{\text{PNSC}}V^- + \frac{\sqrt{3}}{2}b_{\text{PNSC}}V^- \\ -b_{\text{PNSC}}V^+ - \frac{1}{2}b_{\text{PNSC}}V^- - \frac{\sqrt{3}}{2}g_{\text{PNSC}}V^- \\ b_{\text{PNSC}}V^+ - \frac{1}{2}b_{\text{PNSC}}V^- - \frac{\sqrt{3}}{2}g_{\text{PNSC}}V^- \\ g_{\text{PNSC}}V^+ + \frac{1}{2}g_{\text{PNSC}}V^- - \frac{\sqrt{3}}{2}b_{\text{PNSC}}V^- \end{bmatrix}. \quad (42)$$

Applying (32) in (41) gives the abc currents as (43) shown at the bottom of the page.

Calculating the magnitude of each phase results in

$$\begin{bmatrix} |i_a^{F,b}| \\ |i_b^{F,b}| \\ |i_c^{F,b}| \end{bmatrix} = \begin{bmatrix} \sqrt{I_{\alpha,c}^2 + I_{\alpha,s}^2} \\ \sqrt{\left(\frac{-1}{2}I_{\alpha,c} + \frac{\sqrt{3}}{2}I_{\beta,c}\right)^2 + \left(\frac{-1}{2}I_{\alpha,s} + \frac{\sqrt{3}}{2}I_{\beta,s}\right)^2} \\ \sqrt{\left(\frac{-1}{2}I_{\alpha,c} - \frac{\sqrt{3}}{2}I_{\beta,c}\right)^2 + \left(\frac{-1}{2}I_{\alpha,s} - \frac{\sqrt{3}}{2}I_{\beta,s}\right)^2} \end{bmatrix}. \quad (44)$$

Applying the equivalents of $I_{\alpha,c}$, $I_{\alpha,s}$, $I_{\beta,c}$, and $I_{\beta,s}$ from (42) in (44), and replacing g_{PNSC} and b_{PNSC} in (44) with their equivalents from (12) result in

$$\begin{bmatrix} |i_a^{F,b}| \\ |i_b^{F,b}| \\ |i_c^{F,b}| \end{bmatrix} = \frac{1}{(V^+)^2 - (V^-)^2} \begin{bmatrix} \sqrt{N^2 + V^+V^-(Q^2 - P^2 + 2\sqrt{3}PQ)} \\ \sqrt{N^2 + 2V^+V^-(P^2 - Q^2)} \\ \sqrt{N^2 + V^+V^-(Q^2 - P^2 - 2\sqrt{3}PQ)} \end{bmatrix}. \quad (45)$$

This equation gives the expressions of the current magnitudes in three phases for the case in which a fault occurs in phase b . This procedure can be similarly repeated for a fault in phase c . For a fault in phase c , $\delta^+ - \delta^-$ is $-\pi/3$ [32]. Therefore, by assuming $\delta^+ - \delta^- = \lambda^+ - \lambda^- = -\pi/3$ in (36) and performing similar calculations, the expressions of the current magnitudes in the three phases for the faulted phase c (with superscript “ F, c ”) can be obtained as

$$\begin{bmatrix} |i_a^{F,c}| \\ |i_b^{F,c}| \\ |i_c^{F,c}| \end{bmatrix} = \frac{1}{(V^+)^2 - (V^-)^2} \begin{bmatrix} \sqrt{N^2 + V^+V^-(Q^2 - P^2 - 2\sqrt{3}PQ)} \\ \sqrt{N^2 + V^+V^-(Q^2 - P^2 + 2\sqrt{3}PQ)} \\ \sqrt{N^2 + 2V^+V^-(P^2 - Q^2)} \end{bmatrix}. \quad (46)$$

$$\begin{bmatrix} i_a^{F,b} \\ i_b^{F,b} \\ i_c^{F,b} \end{bmatrix} = \begin{bmatrix} I_{\alpha,c} \cos(\lambda^+) + I_{\alpha,s} \sin(\lambda^+) \\ \left(\frac{-1}{2}I_{\alpha,c} + \frac{\sqrt{3}}{2}I_{\beta,c}\right) \cos(\lambda^+) + \left(\frac{-1}{2}I_{\alpha,s} + \frac{\sqrt{3}}{2}I_{\beta,s}\right) \sin(\lambda^+) \\ \left(\frac{-1}{2}I_{\alpha,c} - \frac{\sqrt{3}}{2}I_{\beta,c}\right) \cos(\lambda^+) + \left(\frac{-1}{2}I_{\alpha,s} - \frac{\sqrt{3}}{2}I_{\beta,s}\right) \sin(\lambda^+) \end{bmatrix}. \quad (43)$$

It is clear that the expressions of (39), (45), and (46) are equivalent and that only the order of the expressions is changed based on the faulted phase. Therefore, if

$$\begin{bmatrix} I_1 \\ I_2 \\ I_3 \end{bmatrix} = \frac{1}{(V^+)^2 - (V^-)^2} \begin{bmatrix} \sqrt{N^2 + 2V^+V^-(P^2 - Q^2)} \\ \sqrt{N^2 + V^+V^-(Q^2 - P^2 - 2\sqrt{3}PQ)} \\ \sqrt{N^2 + V^+V^-(Q^2 - P^2 + 2\sqrt{3}PQ)} \end{bmatrix} \quad (47)$$

one can conclude the following:

- 1) If phase a is faulted, $|i_a^{PNSC}| = I_1$, $|i_b^{PNSC}| = I_2$, $|i_c^{PNSC}| = I_3$.
- 2) If phase b is faulted, $|i_a^{PNSC}| = I_3$, $|i_b^{PNSC}| = I_1$, $|i_c^{PNSC}| = I_2$.
- 3) If phase c is faulted, $|i_a^{PNSC}| = I_2$, $|i_b^{PNSC}| = I_3$, $|i_c^{PNSC}| = I_1$.

Depending on the faulted phase, the three expressions of (47) give the current magnitude of the three phases. The first expression of (47), I_1 , always gives the magnitude of the faulted phase. The other two expressions, I_2 and I_3 , calculate the current magnitude of the other two consecutive phases. Therefore, the following equation should be used in order to find the maximum phase current in the PNSC strategy:

$$I_{\max-PNSC} = \max(I_1, I_2, I_3). \quad (48)$$

C. Maximum Phase Currents in ICPS

Since the reference currents generated by the BPSC and PNSC strategies are sinusoidal, the expressions of their maximum instantaneous values can be calculated phase by phase by using the analytical approach. However, due to the non-sinusoidal currents in the ICPS strategy, the I_{\max} expressions for each specific phase cannot be found by using this general analytical approach. Instead, a boundary value limiting all the phase currents in the ICPS strategy is achievable. The reference current of the ICPS strategy is obtained in the $\alpha\beta$ frame by

$$\begin{bmatrix} i_\alpha^{\text{ICPS}} \\ i_\beta^{\text{ICPS}} \end{bmatrix} = \begin{bmatrix} g_{\text{ICPS}}V^+ \cos(\lambda^+) - b_{\text{ICPS}}V^+ \sin(\lambda^+) \\ g_{\text{ICPS}}V^+ \sin(\lambda^+) + b_{\text{ICPS}}V^+ \cos(\lambda^+) \end{bmatrix}. \quad (49)$$

To find the maximum phase current in the abc frame, (32) should be applied in (49) to convert the currents from the $\alpha\beta$ into the abc frame (50) as shown at the bottom of the page.

Expanding g_{ICPS} and b_{ICPS} by using (29) gives

$$\begin{aligned} g_{\text{ICPS}} &= \frac{P}{(V^+)^2 + V^+V^- \cos(\lambda^+ + \lambda^-)} \\ b_{\text{ICPS}} &= \frac{Q}{(V^+)^2 + V^+V^- \cos(\lambda^+ + \lambda^-)}. \end{aligned} \quad (51)$$

Applying (51) in (50) results in

$$\begin{bmatrix} i_a^{\text{ICPS}} \\ i_b^{\text{ICPS}} \\ i_c^{\text{ICPS}} \end{bmatrix} = \frac{1}{V^+ + V^- \cos(\lambda^+ + \lambda^-)} \begin{bmatrix} P \cos(\lambda^+) - Q \sin(\lambda^+) \\ \left(\frac{-1}{2}P + \frac{\sqrt{3}}{2}Q\right) \cos(\lambda^+) + \left(\frac{1}{2}Q + \frac{\sqrt{3}}{2}P\right) \sin(\lambda^+) \\ \left(\frac{-1}{2}P - \frac{\sqrt{3}}{2}Q\right) \cos(\lambda^+) + \left(\frac{1}{2}Q - \frac{\sqrt{3}}{2}P\right) \sin(\lambda^+) \end{bmatrix}. \quad (52)$$

Then, each of the three phase currents can be bounded by an expression as

$$\begin{aligned} |i_a^{\text{ICPS}}| &= \left| \frac{P \cos(\lambda^+) - Q \sin(\lambda^+)}{V^+ + V^- \cos(\lambda^+ + \lambda^-)} \right| \leq \frac{\sqrt{P^2 + Q^2}}{V^+ - V^-} \\ |i_b^{\text{ICPS}}| &= \left| \frac{\left(\frac{-1}{2}P + \frac{\sqrt{3}}{2}Q\right) \cos(\lambda^+) + \left(\frac{1}{2}Q + \frac{\sqrt{3}}{2}P\right) \sin(\lambda^+)}{V^+ + V^- \cos(\lambda^+ + \lambda^-)} \right| \\ &\leq \frac{\sqrt{P^2 + Q^2}}{V^+ - V^-} \\ |i_c^{\text{ICPS}}| &= \left| \frac{\left(\frac{-1}{2}P - \frac{\sqrt{3}}{2}Q\right) \cos(\lambda^+) + \left(\frac{1}{2}Q - \frac{\sqrt{3}}{2}P\right) \sin(\lambda^+)}{V^+ + V^- \cos(\lambda^+ + \lambda^-)} \right| \\ &\leq \frac{\sqrt{P^2 + Q^2}}{V^+ - V^-}. \end{aligned} \quad (53)$$

Although the reference currents generated by the ICPS strategy are unbalanced and non-sinusoidal, the inequalities of (53) are valid for calculating a boundary value that is always greater than all the phase currents. Therefore, the maximum phase current in the ICPS can be bounded by

$$I_{\max-ICPS} = \frac{\sqrt{P^2 + Q^2}}{V^+ - V^-}. \quad (54)$$

$$\begin{bmatrix} i_a^{\text{ICPS}} \\ i_b^{\text{ICPS}} \\ i_c^{\text{ICPS}} \end{bmatrix} = V^+ \cdot \begin{bmatrix} g_{\text{ICPS}} \cos(\lambda^+) - b_{\text{ICPS}} \sin(\lambda^+) \\ \left(\frac{-1}{2}g_{\text{ICPS}} + \frac{\sqrt{3}}{2}b_{\text{ICPS}}\right) \cos(\lambda^+) + \left(\frac{1}{2}b_{\text{ICPS}} + \frac{\sqrt{3}}{2}g_{\text{ICPS}}\right) \sin(\lambda^+) \\ \left(\frac{-1}{2}g_{\text{ICPS}} - \frac{\sqrt{3}}{2}b_{\text{ICPS}}\right) \cos(\lambda^+) + \left(\frac{1}{2}b_{\text{ICPS}} - \frac{\sqrt{3}}{2}g_{\text{ICPS}}\right) \sin(\lambda^+) \end{bmatrix}. \quad (50)$$

V. PROPOSED MAS CONTROL SCHEME

In this paper, the MAS control scheme is proposed for a GCC under unbalanced grid conditions. This scheme is the main contribution of this paper and includes the maximum allowable reactive power (Q_{\max}) delivery (MARPD) and maximum allowable active power (P_{\max}) delivery (MAAPD). Applying the MARPD and MAAPD control schemes to each of the RCG strategies provides the MAS to the grid in terms of voltage and frequency stability/improvement while riding through abnormal conditions and keeping the maximum phase currents limited. The expressions of Q_{\max} and P_{\max} for each of the three RCG strategies are calculated such that the I_{\max} is kept under the pre-set I_{limit} value. This scheme enables two objectives to be achieved simultaneously:

- 1) the maximum allowable active or reactive powers (i.e., P_{\max} and Q_{\max}) can be injected, and
- 2) the maximum phase current can be limited to the pre-set value (i.e., I_{limit}).

In the BPSC strategy, the phase currents are balanced and have equal magnitudes, as obtained in (34). Thus, substituting I_{\max} with I_{limit} in (34) results in finding the Q_{\max} and P_{\max} expressions as

$$Q_{\max}^{\text{BPSC}} = \sqrt{I_{\text{limit}}^2(V^+)^2 - P^2} \quad (55)$$

$$P_{\max}^{\text{BPSC}} = \sqrt{I_{\text{limit}}^2(V^+)^2 - Q^2}. \quad (56)$$

As stated earlier, the ICPS currents contain harmonic components; therefore, conservatively limiting all three phase currents with the boundary found in (54) is a wise idea. By using (54) and substituting I_{\max} with I_{limit} , the equations of the Q_{\max} and P_{\max} in the ICPS strategy are obtained:

$$Q_{\max}^{\text{ICPS}} = \sqrt{I_{\text{limit}}^2(V^+ - V^-)^2 - P^2} \quad (57)$$

$$P_{\max}^{\text{ICPS}} = \sqrt{I_{\text{limit}}^2(V^+ - V^-)^2 - Q^2}. \quad (58)$$

In the previous section, three I_{\max} expressions of (47) were obtained for the three phases in the PNSC strategy. Therefore, Q_{\max} and P_{\max} expressions should be found such that none of the three phase currents exceeds the determined current limitation, I_{limit} . By using (47) and substituting I_{\max} with I_{limit} , the following expressions can be obtained:

$$\begin{bmatrix} Q_1^{\text{PNSC}} \\ Q_2^{\text{PNSC}} \end{bmatrix} = \begin{bmatrix} \frac{\sqrt{I_{\text{limit}}^2[(V^+)^2 - (V^-)^2]^2 - P^2(V^+ + V^-)^2}}{(V^+ - V^-)} \\ \frac{-b + \sqrt{b^2 - 4ac}}{2a} \end{bmatrix} \quad (59)$$

where

$$\begin{cases} a = 3(V^+ + V^-)^2 + (V^+ - V^-)^2 \\ b = 2\sqrt{3}P[(V^+ + V^-)^2 + (V^+ - V^-)^2] \\ c = P^2[(V^+ + V^-)^2 + 3(V^+ - V^-)^2] \\ - 4I_{\text{limit}}^2[(V^+)^2 - (V^-)^2] \end{cases}$$

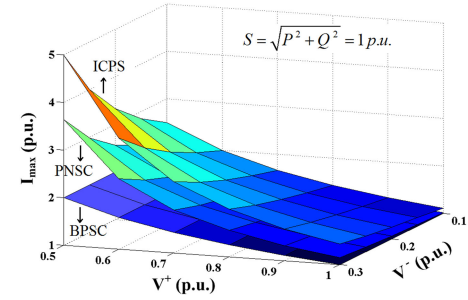


Fig. 2. I_{\max} of three strategies under different V^+ and V^- .

and

$$\begin{bmatrix} P_1^{\text{PNSC}} \\ P_2^{\text{PNSC}} \end{bmatrix} = \begin{bmatrix} \frac{\sqrt{I_{\text{limit}}^2[(V^+)^2 - (V^-)^2]^2 - Q^2(V^+ - V^-)^2}}{(V^+ + V^-)} \\ \frac{-b + \sqrt{b^2 - 4ac}}{2a} \end{bmatrix} \quad (60)$$

where

$$\begin{cases} a = 3(V^+ - V^-)^2 + (V^+ + V^-)^2 \\ b = 2\sqrt{3}Q[(V^+ - V^-)^2 + (V^+ + V^-)^2] \\ c = Q^2[(V^+ - V^-)^2 + 3(V^+ + V^-)^2] \\ - 4I_{\text{limit}}^2[(V^+)^2 - (V^-)^2] \end{cases}$$

By using (59), (60), two different values are obtained for each of the allowable maximum Q and P . Therefore, to have all three phase currents under the limitation, Q_{\max} and P_{\max} should be

$$Q_{\max}^{\text{PNSC}} = \min(Q_1^{\text{PNSC}}, Q_2^{\text{PNSC}}) \quad (61)$$

$$P_{\max}^{\text{PNSC}} = \min(P_1^{\text{PNSC}}, P_2^{\text{PNSC}}). \quad (62)$$

The expressions of the maximum phase currents of the three strategies were obtained in the previous section in (34), (47), and (54). Now, the MAS capability of each strategy can be studied in this section. In order to use the studies in the previous section, it will be helpful to present some conclusions involving the maximum phase currents. The strategies with high maximum phase currents, e.g., the ICPS and PNSC, have less capability to support the grid voltage with an active/reactive power injection compared to the strategies occupying a lower I_{\max} as does the BPSC.

Fig. 2 shows the maximum current of the three strategies under different voltage sag and unbalanced conditions. According to (34), (47), (54) and Fig. 2, the following conclusions can be made:

- 1) The BPSC strategy has the lowest maximum phase current among the studied RCG strategies under the same conditions. Therefore, this strategy has the greatest capability to support the grid voltage/frequency with active or reactive power injections by the MARPD and MAAPD control schemes. This capability will be

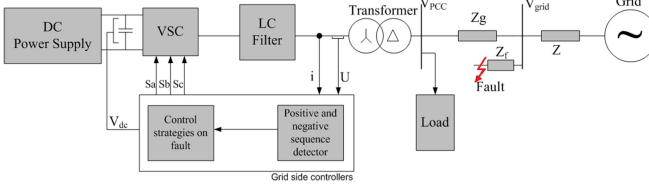
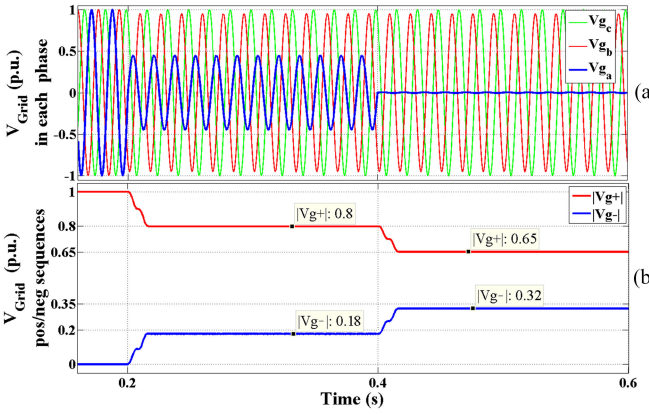


Fig. 3. Circuit topology of the grid-connected converter.

Fig. 4. Emulated fault: (a) abc grid voltages, (b) positive and negative-sequences of the grid voltage.

also shown by simulation and experimental results in Sections VI and VII.

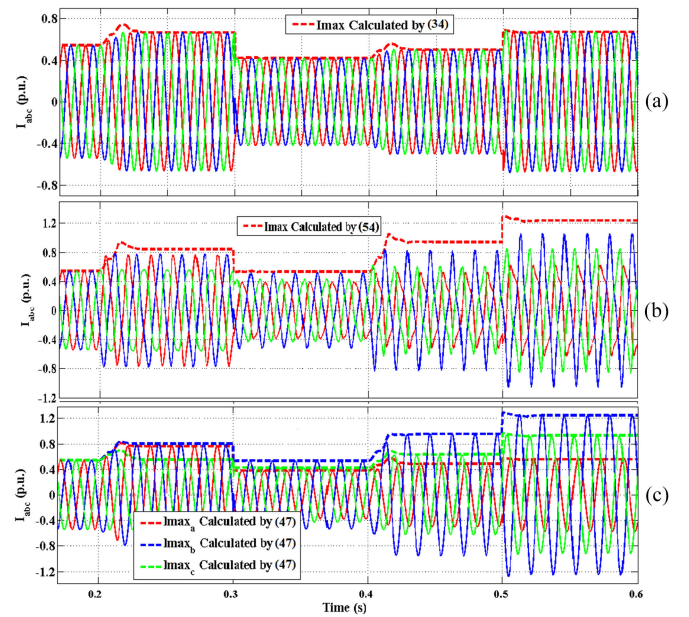
- 2) The PNSC strategy ranks second in terms of current magnitudes under unbalanced voltage conditions. Thus, the effectiveness of its MAS scheme is less than that of the BPSC strategy because the PNSC strategy has less room for the MAAPD or MARPD control scheme to inject additional active or reactive currents.
- 3) The ICPS strategy has the greatest phase currents among the three strategies. Obviously, less improvement is expected for this strategy after applying the MAAPD or MARPD scheme.

VI. SIMULATION RESULTS

To verify the mathematical analysis and demonstrate the effectiveness of the proposed methods, three test cases are studied and implemented in this section. Fig. 3 illustrates the circuit topology of a grid-connected 2.2 MVA, 690 V, 60 Hz converter-interfaced DG unit. The ac voltage source (grid) and the indicated fault in Fig. 3 realize the desired voltage dip presented in Fig. 4. A dc power supply can be used to realistically emulate the renewable energy resources and storage in the dc-link [30]. This assumption is widely used in most studies [21]–[25]. The proportional-resonant (PR) control is used in the α/β reference frame for the converter current regulation. It is also assumed that a type B fault (phase a to ground) [31] occurs with moderate and severe voltage dips in phase a , as indicated in Fig. 4. The simulation system parameters are listed in Table I.

TABLE I
TEST SYSTEM PARAMETERS—CASE A

$P^*(t_0 - t_3 : 0 - 0.3\text{s})$	1 MW	$Q^*(t_0 - t_7 : 0 - 0.5\text{s})$	0.7 MVAR
$P^*(t_3 - t_9 : 0.3 - 0.6\text{s})$	0.3 MW	$Q^*(t_7 - t_9 : 0.5 - 0.6\text{s})$	1 MVAR
$Z_g (\text{m}\Omega)$	$34.6 \angle 78.3^\circ$	$V_{\text{DC}} (\text{V})$	2000
$Z_L (\text{m}\Omega)$	$37.8 \angle 87^\circ$	$V_{L-L, \text{RMS}} (\text{V})$	690
$Z_f (t_1 - t_5 : 0.2 - 0.4\text{s})$	$0.8 \text{ m}\Omega$	$f(\text{Hz})$	60
$Z_f (t_5 - t_{10} : 0.4 - 0.65\text{s})$	0	$S (\text{MVA})$	2.2

Fig. 5. Calculation of I_{max} values by (34), (47), and (54) versus simulation results for (a) BPSC, (b) ICPS, and (c) PNSC strategies.

A. Test Case A: Maximum Phase Currents, Calculation Versus Simulation

This section presents the simulation results for each RCG strategy under different grid fault scenarios in order to compare these results with those for the obtained analytical expressions of (34), (47), and (54). Between $t_1 = 0.2$ s and $t_3 = 0.4$ s, a moderate voltage dip happens where $V_g^+ = 0.8$ p.u. and $V_g^- = 0.18$ p.u. as indicated in Fig. 4. In addition, for more evaluations, a severe voltage dip is also emulated between $t_3 = 0.4$ s and $t_5 = 0.6$ s, where $V_g^+ = 0.65$ p.u. and $V_g^- = 0.32$ p.u. as shown in Fig. 4. In this test case, P^* is set to be 1 MW until $t_2 = 0.3$ s and 0.3 MW after t_2 . Also, Q^* is set to be 0.7 MVAR until $t_4 = 0.5$ s and 1 MVAR after t_4 . Therefore, there are four different fault conditions. Fig. 5 illustrates the simulation results for the BPSC, ICPS and PNSC strategies under these four conditions. Relatively lower currents of the BPSC strategy and higher currents of ICPS can be observed in Fig. 5(a) and (b) in agreement with the conclusions and discussions in Sections IV and V. As it is indicated in Fig. 5(b), the I_{max} has a small inaccuracy after $t_5 = 0.4$ s that is due to its non-sinusoidal reference currents. By using (47), the I_{max} for each phase in PNSC is accurately calculated. The results are shown in Fig. 5(c).

TABLE II
SPECIFIED ACTIVE POWER AND I_{limit} COMMANDS—CASE B

$P^*(t_0 - t_3 : 0 - 0.4\text{s})$	1 MW	$P^*(t_3 - t_6 : 0.4 - 0.7\text{s})$	0.3 MW
$I_{\text{limit}}^*(t_2 - t_5 : 0.3 - 0.6\text{s})$	0.9 p.u.	$I_{\text{limit}}^*(t_5 - t_6 : 0.6 - 0.7\text{s})$	1.2 p.u.
$Z_f(t_1 - t_4 : 0.2 - 0.5\text{s})$	0.8 mΩ	$Z_f(t_4 - t_6 : 0.5 - 0.7\text{s})$	0

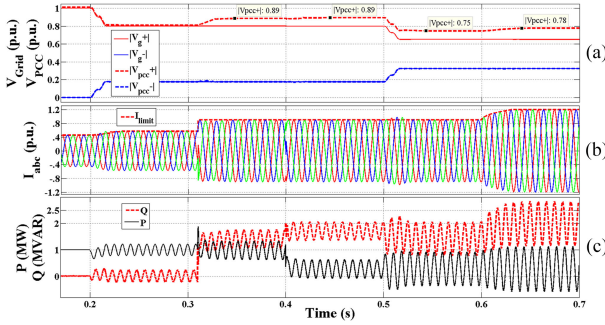


Fig. 6. Case B—BPSC strategy: (a) pos/neg-sequences of grid and PCC voltages, (b) injected currents, (c) p and q .

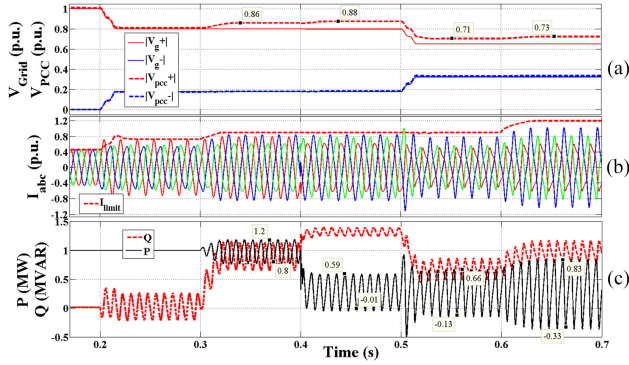


Fig. 7. Case B—ICPS strategy: (a) pos/neg-sequences of grid and PCC voltages, (b) injected currents, (c) p and q .

B. Test Case B: Maximum Phase Current Limitation and MARPD Control Scheme

This section tests and studies the MARPD equations and presents the simulation results for each RCG strategy with the MARPD method under different fault conditions. The grid voltage deteriorates with positive and negative values similar to those in Case A for both moderate and severe faults. Moreover, P^* is set to be 1 MW until $t_3 = 0.4\text{s}$ and 0.3 MW after t_3 . The MARPD method is applied in order to support the grid voltage under the fault after $t_2 = 0.3\text{s}$, which respects the specified maximum current limitation, I_{limit} (0.9 p.u. until $t_5 = 0.6\text{s}$ and 1.2 p.u. after t_5). These reference commands are summarized in Table II. Therefore, there are four different fault conditions, where the proposed MARPD method is examined. Three main observations are expected after applying the MARPD equations in each strategy:

- 1) The current injected by each strategy should respect the pre-set values of I_{limit} (part ‘b’ of Figs. 6, 7, and 8).
- 2) The positive sequence value of the voltage should have the maximum increase with respect to the reference active

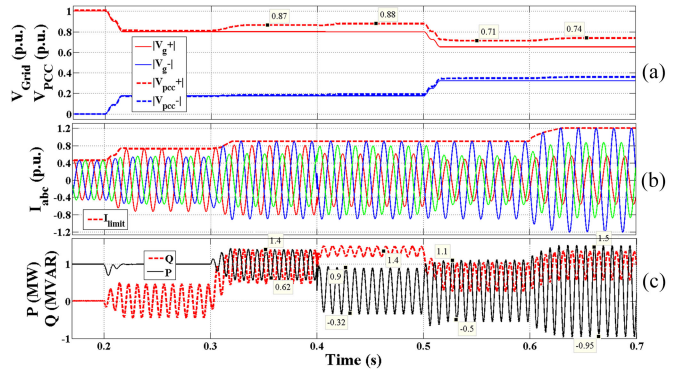


Fig. 8. Case B—PNSC strategy: (a) pos/neg-sequences of grid and PCC voltages, (b) injected currents, (c) p and q .

power and pre-set I_{limit} values in each strategy (part ‘a’ of Figs. 6, 7, and 8).

- 3) The maximum deliverable reactive power is obtained for each strategy by using the MARPD equations to satisfy the previous two objectives, i.e., current limitation and maximum voltage boost (part ‘c’ of Figs. 6, 7, and 8).

Fig. 6 demonstrates the simulation results for the BPSC strategy in test case B. As Fig. 6(b) shows, the injected balanced currents are limited to I_{limit}^* by calculating the maximum allowable reactive power obtained in (55). Fig. 6(a) reveals the positive PCC voltage boost, which is more than that of the other two strategies. As is stated in Section V, the BPSC strategy has the greatest capability among the RCG strategies to support the PCC voltage under the same condition. The voltage boost is the most (i.e., 0.13 p.u.) from t_5 to t_6 , where I_{limit}^* is 1.2 p.u., and the reference active power is only 0.3 MW. Furthermore, the value of the oscillations on the instantaneous active power in the BPSC (i.e., \tilde{p}_{max} reaches 0.8 MW after t_5) is more than that of the previous strategies. Fig. 7 illustrates the simulation results for the ICPS strategy in the test case B. As Fig. 7(b) shows, the injected non-sinusoidal currents are equal to or less than I_{limit}^* by applying the MARPD formula for the ICPS strategy presented in (57). As Fig. 7(c) illustrates, the maximum allowable reactive power is obtained successfully for each of the four fault conditions. Fig. 7(a) reveals the positive PCC voltage boost, which is less than that of the BPSC strategy under the same conditions. The voltage boost is 0.08 p.u. from t_3 to t_4 and from t_5 to t_6 . Fig. 8 shows the simulation results of the PNSC strategy in test case B. As Fig. 8(a) shows, the voltage has been increased by 0.09 p.u. whereas the injected unbalanced currents are limited to the I_{limit}^* by applying the MARPD equation presented in (61). Table III summarizes the improvements after applying the proposed MARPD method. According to Table III, applying the proposed MAS scheme in the BPSC resulted in a +20% voltage improvement, while the improvements in the PNSC and ICPS strategies were +14% and +12%, respectively.

C. Test Case C: Grid Code Requirement (GCRs) on Q Injection, Maximum Current Limitation and MAAPD Scheme

In this test case, the GCC provides the reactive current mandated by fault ride-through GCRs, which require injecting 2%

TABLE III
SUMMARY OF THE RESULTS OF THE PROPOSED MARPD EQUATIONS: VOLTAGE IMPROVEMENTS IN FOUR CONDITIONS OF TEST CASE B

Positive voltage boost ups in p.u.					
	Cond. 1 0.3–0.4 s	Cond. 2 0.4–0.5 s	Cond. 3 0.5–0.6 s	Cond. 4 0.6–0.7 s	Maximum voltage improvements in %
BPSC	+0.09	+0.09	+0.10	+0.13	20%
ICPS	+0.06	+0.08	+0.06	+0.08	12%
PNSC	+0.07	+0.08	+0.06	+0.09	14%

reactive current for each 1% of the voltage dip, up to a maximum of 100% of the rated current [6]. The two moderate and severe fault cases in Fig. 4 are tested here. According to the GCRs, the GCC should inject 0.4 p.u. and 0.7 p.u. reactive current/power, respectively, under the moderate and severe faults (0.2 p.u. and 0.35 p.u. voltage drops) and curtail the active power. In normal operation, the GCC could inject 0.92 p.u. active and 0.4 p.u. reactive currents/powers (i.e., $S = 1$ p.u.). However, these results do not occur under the fault since the fault current obtained from $S = 1$ p.u. exceeds its rated value, causing protection trip and low voltage ride through (LVRT) failure. Therefore, by using the MAAPD control scheme, one can obtain the maximum allowable active power (in each strategy), which simultaneously respects the fault current limitation. Fig. 9 shows the maximum allowable active power values [obtained by (56), (58), and (62)] for each strategy under two fault scenarios.

For instance, the maximum allowable active power values with the BPSC strategy under the moderate fault are calculated to be 0.69 p.u. and 0.87 p.u. when the I_{limit} values are, respectively, 1 p.u. and 1.2 p.u. (by using the MAAPD equations presented in Section V). As demonstrated in Fig. 9, the RCG strategies should curtail the active power to respect the fault current limitation and avoid the protection tripping. However, even with the zero active power injection under the severe fault condition, the ICPS and PNSC strategies are not able to inject 0.7 p.u. reactive power without exceeding I_{limit} , as indicated in Fig. 9, and can be analytically proven by (57) and (59). On the other hand, the BPSC strategy can provide the required reactive powers and simultaneously obey the fault current limitation as indicated in Fig. 9(a). This result is also theoretically obtained by (55).

VII. EXPERIMENTAL RESULTS

For further verification of the analytical expressions and evaluation of the proposed schemes, an experimental test system, demonstrated in Fig. 10, is employed. The experimental system consists of a VSC connected to a 60 Hz, 208 V grid via an interfacing transformer, and operating in the PQ mode. A Semistack intelligent power module consisting of gate drives and six insulated gate bipolar transistors is used to implement the GCC. The switching frequency is 10 kHz and the maximum converter current is set to 10 A. The parameters of the test system are reported in Table IV. The converter is interfaced to a dSPACE1104 board via a CMOS/TTL interfacing circuit. The proposed MAS schemes along with the presented RCG

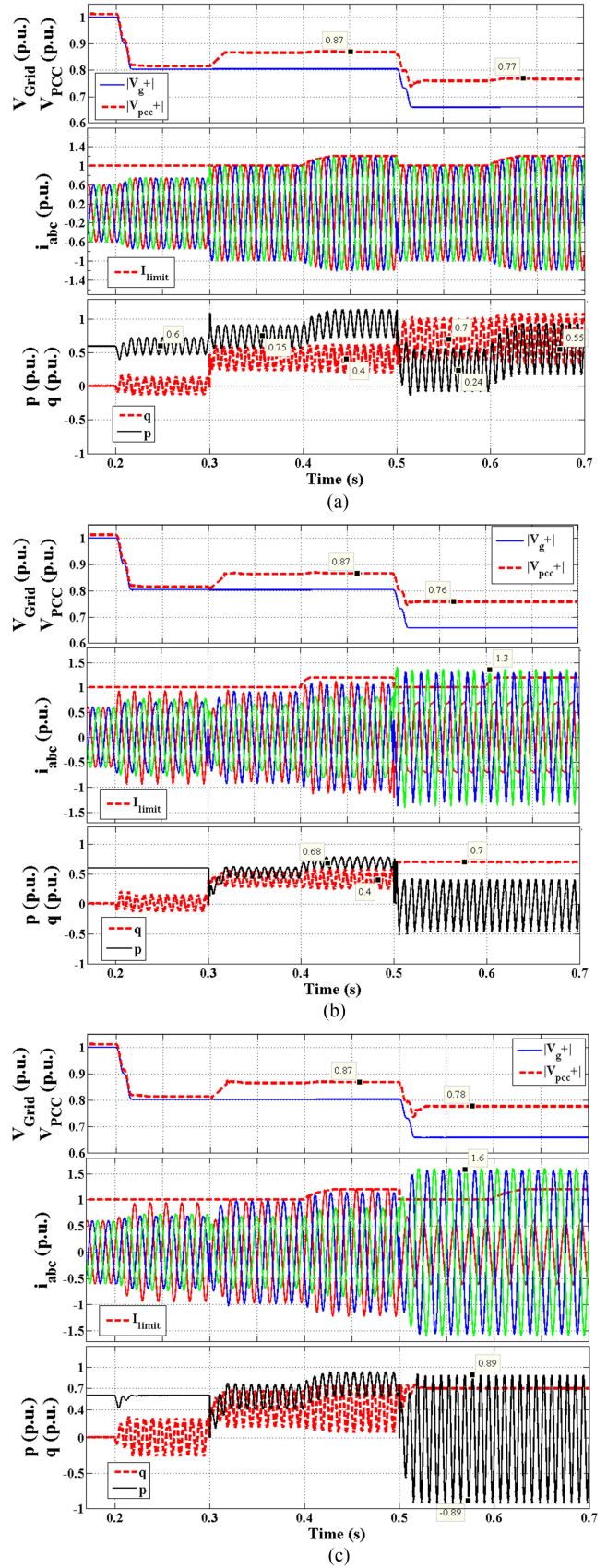


Fig. 9. Case C—magnitudes of pos-sequence grid and PCC voltages, injected currents, p and q of (a) BPSC; (b) ICPS; (c) PNSC strategies.

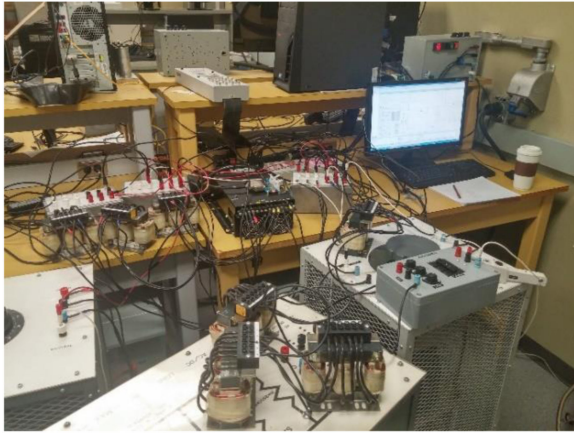


Fig. 10. Test setup.

TABLE IV
EXPERIMENTAL TEST SYSTEM PARAMETERS

Z_g	$j2\pi f \times 4.9 \text{ m}\Omega$	Z	$j2\pi f \times 1.2 \text{ m}\Omega$
Z_{filter}	$j2\pi f \times 1.2 \text{ m}\Omega$	$I_{\text{rated}} = I_{\text{limit}}$	10 A
Z_{fault}	$j2\pi f \times 7.7 \text{ m}\Omega$	f	60 Hz

strategies are implemented on the board for switching signal generation. The control system code is generated by the Real-Time-WorkShop toolbox in MATLAB/Simulink. The proposed control schemes are designed by following the detailed procedure presented in Sections II and V. The results of the selected test cases are reported as follows.

A. Experimental Test Case A: BPSC, ICPS and PNSC

This test case is a basic test to verify the analytical studies of this paper. In this test case, $Q = 140 \text{ VAr}$ is injected by the GCC. An unbalanced fault is emulated via a fault impedance ($Z_{\text{fault}} = j2\pi f \times 7.7 \text{ m}\Omega$) and a circuit breaker, which make the short circuit between phase a and the ground of the system. Fig. 11(a) shows the positive and negative sequences of the voltage during the fault between $t = 1.7 \text{ s}$ and $t = 4.7 \text{ s}$. Before the fault occurrence, all strategies produce similar abc currents with the amplitude of 4 A. However, the behavior of the currents of the three strategies significantly vary during the unbalanced fault. According to the experimental results of the faulted period, shown in Fig. 11, the amplitude of the maximum phase currents are 5.2 A, 7 A, and 6.3 A for the BPSC, ICPS and PNSC strategies, respectively. Table V compares the experimental results for the I_{\max} values with the values calculated by using the expressions derived in Section IV. Table V verifies the accuracy of the analytical expressions.

B. Experimental Test Case B: GCR Versus MARPD

This test case aims to compare the results of two schemes: GCR and MARPD. In this test case, $P = 225 \text{ W}$ is injected by the GCC as indicated in Fig. 12(c). Again, the similar phase-to-ground fault occurs at $t = 1.5 \text{ s}$, as Fig. 12(a) reveals. The PCC

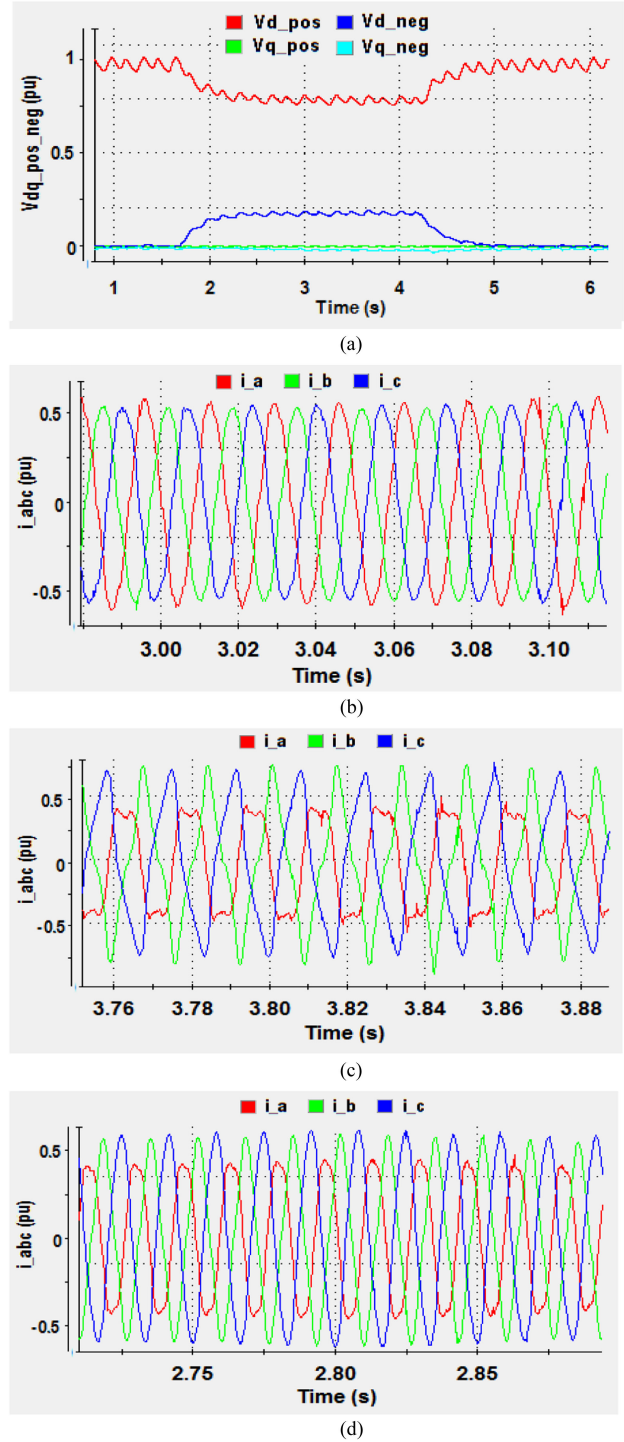


Fig. 11. Experimental results of test case A: (a) faulted PCC voltage, (b) currents with BPSC, (c) currents with ICPS, and (d) currents with PNSC.

voltage profiles drops from 1 p.u. to 0.84 p.u. From $t = 5 \text{ s}$ to $t = 9.3 \text{ s}$, the GCR scheme is activated, boosting the voltage to 0.87 p.u. At $t = 9.3 \text{ s}$, the MARPD scheme with $I_{\text{limit}} = 10 \text{ A}$ is activated. As Fig. 12(a) indicates, the PCC voltage is increased to 0.97 p.u. The limitations of the converter are not violated, and the applied method respects the imposed predefined $I_{\text{limit}} = 10 \text{ A}$ as indicated in Fig. 12(b).

TABLE V
COMPARISON BETWEEN MATHEMATICAL AND EXPERIMENTAL RESULTS
FOR I_{\max} VALUES UNDER THE FAULT

Mathematical Expressions in Section IV	Experimental Results
$I_{\max -BPSC}$	5.2 A
$I_{\max -ICPS}$	7 A
$I_{\max -a-PNSC}$	4.1 A
$I_{\max -b-PNSC}$	6.3 A
$I_{\max -c-PNSC}$	6.3 A

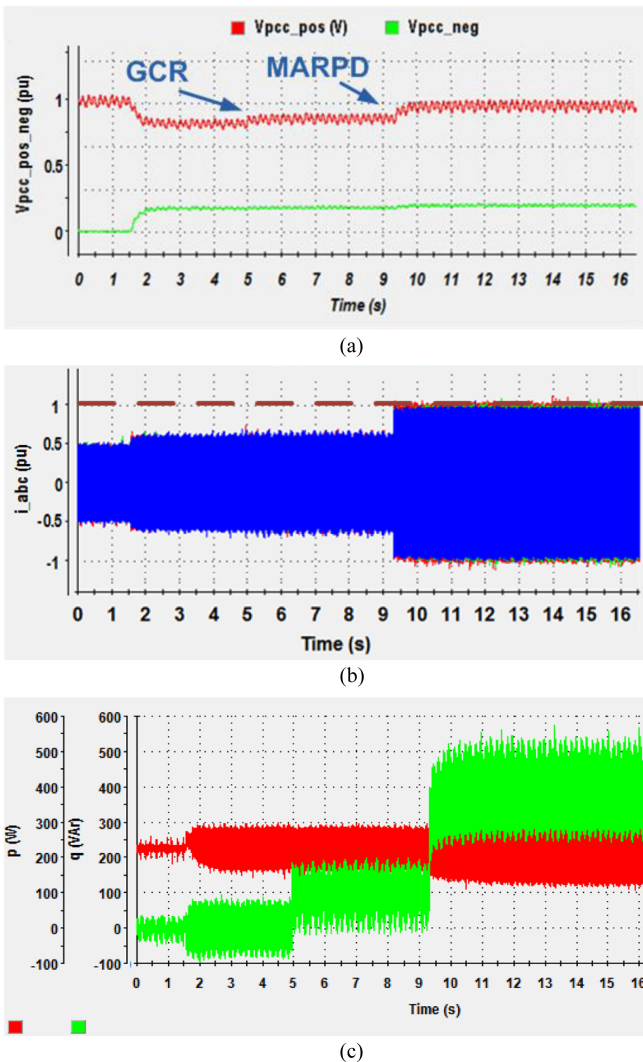


Fig. 12. Experimental results of test case B—MARPD versus GCR: (a) faulted PCC voltage, (b) inverter currents, (c) instantaneous active/reactive powers.

VIII. DISCUSSION

System operators can use the results obtained from the comparative studies in this paper. As mentioned in the previous sections, different aspects of the LVRT-RCG strategies can be assessed. Their behaviours in the normal operation are the same. However, different distinguishing characteristics arise under the low voltage or unbalanced conditions. Therefore, they should be evaluated based on different characteristics such as the har-

monic content, complexity of the controller, maximum oscillations on the instantaneous active/reactive power, maximum instantaneous phase current, maximum allowable grid support, and maximum voltage depth in which each strategy can still meet GCRs. These are the main contributions of this paper.

According to the analytical expressions of the maximum fault currents, presented in Section IV, the BPSC strategy has the lowest fault current, and the ICPS has the highest. Therefore, the BPSC strategy has more capability for injecting additional active or reactive powers with the proposed MAAPD and MARPD methods. Consequently, the MAS scheme theoretically leads to the highest improvement if it is applied in the BPSC strategy. The MAS equations also reveal that when the BPSC strategy is applied in the GCC, the maximum supportable voltage sag is much higher comparing to the cases when the other two strategies are applied. The maximum supportable voltage sag is the maximum depth of the faulted voltage where the GCRs are still met. These analytical conclusions about the maximum fault current are also verified with the simulation and experimental results, and are quantitatively compared in Tables III and V.

As a second contribution, this paper has also compared the results of the three strategies in terms of power oscillations and fault current magnitudes. For example, according to the results obtained in Sections III and IV, the superior behaviour of ICPS and BPSC in terms of the power oscillations, and the superior behaviour of BPSC in terms of the current, have been theoretically demonstrated. In future work, these comparative studies can be performed for the other existing strategies. These comparisons and conclusions will help system operators to select the proper RCG strategy from the existing ones.

IX. CONCLUSION

This paper presented the analytical evaluations and mathematical assessments of three RCG strategies in grid-connected converter-interfaced DG units. The three most important parameters of these strategies were studied for evaluation and comparison purposes. Based on the obtained formulas for the maximum phase currents, the MAS control schemes were proposed for each of the three strategies. The proposed methods provide the maximum allowable voltage/frequency support by injecting the maximum allowable reactive/active power while simultaneously respecting the converter current limitations. These advantages will simultaneously benefit the system operators and the DG owners under fault conditions. The simulation results for different selected fault test cases and various reference commands were reported for each strategy and showed the accuracy and effectiveness of the proposed formulas. This paper will be helpful for evaluating the performances of RCG strategies, eliminating their existing drawbacks, exploiting the maximum utilization out of each, and improving them. In addition, the ideas in this paper can be applied to other RCG strategies.

REFERENCES

- [1] M. F. M. Arani and Y. A. R. I. Mohamed, "Analysis and performance enhancement of vector-controlled VSC in HVDC links connected to very weak grids," *IEEE Trans. Power Syst.*, vol. PP, no. 99, pp. 1–10, doi: 10.1109/TPWRS.2016.2540959.

- [2] F. Blaabjerg, M. Liserre, and K. Ma, "Power electronics converters for wind turbine systems," *IEEE Trans. Ind. Appl.*, vol. 48, no. 2, pp. 708–719, Mar./Apr. 2012.
- [3] D. Xie, Z. Xu, L. Yang, Ostergaard, Y. Xue, and K. Wong, "A comprehensive LVRT control strategy for DFIG wind turbines with enhanced reactive power support," *IEEE Trans. Power Syst.*, vol. 28, no. 3, pp. 3302–3310, Aug. 2013.
- [4] M. F. M. Arani and Y. A. R. I. Mohamed, "Assessment and enhancement of a full-scale PMSG-Based wind power generator performance under faults," *IEEE Trans. Energy Convers.*, vol. 31, no. 2, pp. 728–739, Jun. 2016.
- [5] A. Moawwad, M. Shawky El M, and W. Xiao, "A novel transient control strategy for VSC-HVDC connecting offshore wind power plant," *IEEE Trans. Sustain. Energy*, vol. 5, no. 4, pp. 1056–1069, Oct. 2014.
- [6] S. Alaraifi, A. Moawwad, M. Shawky, E. Moursi, and V. Khadkikar, "Voltage booster schemes for fault Ride-Through enhancement of variable speed wind turbines," *IEEE Trans. Sustain. Energy*, vol. 4, no. 4, pp. 1071–1081, Oct. 2013.
- [7] S. Rijke, H. Ergun, D. Hertem, and J. Driesen, "Grid impact of voltage control and reactive power support by wind turbines equipped with direct-drive synchronous machines," *IEEE Trans. Sustain. Energy*, vol. 3, no. 4, pp. 890–898, Oct. 2012.
- [8] S. S. Smater and A. D. Dominguez-Garcia, "A framework for reliability and performance assessment of wind energy conversion systems," *IEEE Trans. Power Syst.*, vol. 26, no. 4, pp. 2235–2245, Nov. 2011.
- [9] S. K. Chaudhary, R. Teodorescu, P. Rodriguez, P. C. Kjaer, and A. M. Gole, "Negative sequence current control in wind power plants with VSC-HVDC connection," *IEEE Trans. Sustain. Energy*, vol. 3, no. 3, pp. 2235–2245, Jul. 2012.
- [10] S. Seman, J. Niiranen, and A. Arkkio, "Ride-through analysis of doubly fed induction wind-power generator under unsymmetrical network disturbance," *IEEE Trans. Power Syst.*, vol. 21, no. 4, pp. 1782–1789, Nov. 2006.
- [11] H. M. Hasanien and S. M. Muyeen, "Design optimization of controller parameters used in variable speed wind energy conversion system by genetic algorithms," *IEEE Trans. Sustain. Energy*, vol. 3, no. 2, pp. 200–208, Apr. 2012.
- [12] A. P. Grilo, A. D. A. Mota, L. T. M. Mota, and W. Freitas, "An analytical method for analysis of large-disturbance stability of induction generators," *IEEE Trans. Power Syst.*, vol. 22, no. 4, pp. 1861–1869, Nov. 2007.
- [13] J. Chen, L. Jiang, W. Yao, and Q. H. Wu, "Perturbation estimation based nonlinear adaptive control of a full-rated converter wind turbine for fault ride-through capability enhancement," *IEEE Trans. Power Syst.*, vol. 29, no. 6, pp. 2733–2743, Nov. 2014.
- [14] S. Muyeen, R. Takahashi, T. Murata, and J. Tamura, "A variable speed wind turbine control strategy to meet wind farm grid code requirements," *IEEE Trans. Power Syst.*, vol. 25, no. 1, pp. 331–340, Feb. 2010.
- [15] G. Delille, B. François, and G. Malarange, "Dynamic frequency control support by energy storage to reduce the impact of wind and solar generation on isolated power system's inertia," *IEEE Trans. Sustain. Energy*, vol. 3, no. 4, pp. 931–939, Oct. 2012.
- [16] Y. Bae, T. Vu, and R. Kim, "Implemental control strategy for grid stabilization of Grid-connected PV system based on german grid code in symmetrical low-to-medium voltage network," *IEEE Trans. Energy Convers.*, vol. 28, no. 3, pp. 619–631, Sep. 2013.
- [17] A. Hajizadeh, M. A. Golkar, and A. Feliachi, "Voltage control and active power management of hybrid fuel-cell/energy-storage power conversion system under unbalanced voltage sag conditions," *IEEE Trans. Energy Convers.*, vol. 25, no. 4, pp. 1195–1208, Dec. 2010.
- [18] T. Vrionis, X. Koutiva, N. Vovos, and G. B. Giannakopoulos, "Control of an HVdc link connecting a wind farm to the grid for fault ride-through enhancement," *IEEE Trans. Power Syst.*, vol. 22, no. 4, pp. 2039–2047, Nov. 2007.
- [19] C. Feltes, H. Wrede, F. W. Koch, and I. Erlich, "Enhanced fault ride-through method for wind farms connected to the grid through VSC-based HVDC transmission," *IEEE Trans. Power Syst.*, vol. 24, no. 3, pp. 1537–1546, Aug. 2009.
- [20] L. Xu, L. Yao, and C. Sasse, "Grid integration of large DFIG-Based wind farms using VSC transmission," *IEEE Trans. Power Syst.*, vol. 22, no. 3, pp. 976–984, Aug. 2007.
- [21] R. Teodorescu *et al.*, *Grid Converters for Photovoltaic and Wind Power Systems*. New York, NY, USA: Wiley, 2011.
- [22] P. Rodriguez, A. V. Timbus, R. Teodorescu, M. Liserre, and F. Blaabjerg "Flexible active power control of distributed power generation systems during grid faults," *IEEE Trans. Ind. Electron.*, vol. 54, no. 5, pp. 2583–2592, Oct. 2007.
- [23] K. Ma, W. Chen, M. Liserre, and F. Blaabjerg, "Power controllability of three-phase converter with unbalanced AC source," *IEEE Trans. Power Electron.*, vol. 30, no. 3, pp. 1591–1604, Mar. 2015.
- [24] A. Camacho, M. Castilla, J. Miret, J. Vasquez, and E. Alarcon-Gallo "Flexible voltage support control for three-phase distributed generation inverters under grid fault," *IEEE Trans. Ind. Electron.*, vol. 60, no. 4, pp. 1429–1441, Apr. 2013.
- [25] X. Guo, X. Zhang, B. Wang, W. Wu, and J. M. Guerrero, "Asymmetrical grid fault ride-through strategy of three-phase grid-connected inverter considering network impedance impact in low-voltage grid," *IEEE Trans. Power Electron.*, vol. 29, no. 3, pp. 1064–1068, Mar. 2014.
- [26] H. Akagi, E. H. Watanabe, and M. Aredeas, *Instantaneous Power Theory and Applications to Power Conditioning*. New York, NY, USA: The Institute of Electrical and Electronics Engineers, Inc., 2007.
- [27] M. Aredeas, H. Akagi, E. H. Watanabe, E. V. Salgado, and L. F. Encarnacao, "Comparisons between the p-q and p-q-r theories in three-phase four-wire systems," *IEEE Trans. Power Electron.*, vol. 24, no. 4, pp. 924–933, Apr. 2009.
- [28] *Interconnection of Distributed Resources and Electricity Supply Systems*, CSA Std. C22.3 No. 9-08, Feb. 2009.
- [29] C. Liu, D. Xu, N. Zhu, F. Blaabjerg, and M. Chen, "DC-voltage fluctuation elimination through DC-capacitor current control for DFIG Converters under unbalanced grid voltage conditions," *IEEE Trans. Power Electron.*, vol. 28, no. 7, pp. 3206–3218, Jul. 2013.
- [30] M. M. Shabestary, "A comparative analytical study on low-voltage ride-through reference-current-generation (LVRT-RCG) strategies in converter-interfaced DER units," M.S. thesis, Univ. Alberta, Edmonton, AB, Canada, 2015.
- [31] G. Saccomando, J. Svensson, and A. Sannino, "Improving voltage disturbance rejection for variable-speed wind turbines," *IEEE Trans. Energy Convers.*, vol. 17, no. 3, pp. 422–428, Sep. 2002.
- [32] J. Miret, A. Camacho, M. Castilla, L. García de Vicuna, and J. Matas, "Control schemewith voltage support capability for distributed generation inverters under voltage sags," *IEEE Trans. Power Electron.*, vol. 28, no. 11, pp. 5252–5262, Nov. 2013.
- [33] A. Junyent-Ferre, O. Gomis-Bellmunt, T. C. Green, and D. E. Soto-Sánchez, "Current control reference calculation issues for the operation of renewable source grid interface VSCs under unbalanced voltage sags," in *IEEE Trans. Power Electron.*, vol. 26, no. 12, pp. 3744–3753, Dec. 2011.



Masoud M. Shabestary (S'14) received the B.Sc. degree in electrical engineering from the Amirkabir University of Technology (Tehran Polytechnic), Tehran, Iran, in 2011, and the M.Sc. degree in energy systems from the University of Alberta, Edmonton, AB, Canada, in 2015. He is currently working toward the Ph.D. degree in electrical engineering at the University of Alberta. From 2011 to 2013, he served as a Research Assistant at the FACTS Laboratory, Amirkabir University of Technology, Tehran, Iran. His research interests include renewable energies and distributed generation units, their analysis, control and protection, and application of power converters in hybrid smart microgrids.



Yasser Abdel-Rady I. Mohamed (M'06–SM'011) was born in Cairo, Egypt, on November 25, 1977. He received the B.Sc. (Hons.) and M.Sc. degrees in electrical engineering from the Ain Shams University, Cairo, Egypt, in 2000 and 2004, respectively, and the Ph.D. degree in electrical engineering from the University of Waterloo, Waterloo, ON, Canada, in 2008. He is currently with the Department of Electrical and Computer Engineering, University of Alberta, AB, Canada, as an Associate Professor. His research interests include dynamics and controls of power converters; grid integration of distributed generation and renewable resources; microgrids; modeling, analysis and control of smart grids; electric machines and motor drives.

He is an Associate Editor of the IEEE TRANSACTIONS ON INDUSTRIAL ELECTRONICS, and an Editor of the IEEE TRANSACTIONS ON POWER SYSTEMS and IEEE TRANSACTIONS ON SMART GRID. He is a registered Professional Engineer in the Province of Alberta.